Journal of Applied Geophysics 191 (2021) 104376

Contents lists available at ScienceDirect

Journal of Applied Geophysics

journal homepage: www.elsevier.com/locate/jappgeo

The reliability of muography applied in the detection of the animal burrows within River Levees validated by means of geophysical techniques

G. Baccani [a,b], L. Bonechi [b], M. Bongi [a,b], N. Casagli [c,d], R. Ciaranfi [b], V. Ciulli [a,b], R. D'Alessandro [a,b], S. Gonzi [a], L. Lombardi [c], S. Morelli [c], M. Nocentini [c], V. Pazzi [c,*], C. Tacconi Stefanelli [c], L. Viliani [b]

[a] Department of Physics and Astronomy, University of Florence, Italy
[b] INFN, Unit of Florence, Italy
[c] Department of Earth Science, University of Florence, Italy
[d] National Institute of Oceanography and Applied Geophysics - OGS, Trieste, Italy

ARTICLE INFO

Article history:
Received 10 September 2020
Received in revised form 15 March 2021
Accepted 18 May 2021
Available online 21 May 2021

Keywords:
Muons
Cosmic ray
ERT
Electrical resistivity
Riverbanks monitoring

ABSTRACT

Animal burrows in a river's earthen levee leads to water piping phenomena causing structural damage and eventual collapse during floods. Currently, the state of the art comprises case studies that deal with management and maintenance, while very few documents attempt at assessing possible animal-induced failure mechanisms. For the latter, detection and characterisation of the animal burrows is crucial and Electrical Resistivity Tomography (ERT) and Ground Penetrating Radar are the most employed geophysical techniques. Between 2017 and 2018 a team of physicists, engineering geologists, and geophysicists has for the first time probed the possibility of exploiting the Muon Transmission Radiography (MTR) to verify the internal conservation status of levees that were visibly damaged by animal activities. The technique is a non-invasive method, currently under development, based on the detection of muons, a highly penetrating component of atmospheric cosmic rays. MTR is capable of providing angular maps of the average density of the material present in front of the detector. A test site measurement campaign was carried out with a prototype instrument placed at the side of the levee. This new survey methodology was compared to a more traditional ERT measurement, performed with a pole-dipole and dipole-dipole configuration. Moreover, the actual burrows' distribution was mapped during the demolition works using Terrestrial Laser Scanner measurements to validate and constrain results. The comparison between ERT and MTR maps shows that, in spite of some limitations, the latter is a suitable and promising technique that could successfully complement a program of geological risk assessment.

1. Introduction

River levees, thanks to their position between water channels and floodplains, have an important role in flood control, especially artificial ones that are designed to protect crops, buildings, and structures as well as human settlements (Brierley et al., 1997; Fishera et al., 2017; Pazzi et al., 2017; Morelli et al., 2020). Unfortunately, there are many instances where a river's earthen levee system has not been structurally preserved and may suffer functional damages. This may be due to alterations in the internal structures (material degradation or internal erosion leading to loss of properties) and/or instability processes both on the inner and outer slopes (Perri et al., 2014; Fishera et al., 2017; Pazzi et al., 2017; Bièvre et al., 2018; Morelli et al., 2020). The deferred or not adequately proportioned maintenance over time, sometimes leads to a progressive porosity variation through all the levee body, that grows to such an extent as to cause visible cracks and fissures on the external surfaces (Borgatti et al., 2017; Fishera et al., 2017). This deterioration can lead to an increase of water infiltration (both from high water levels in the river and persistent rainfalls) and thus an irregular saturation that can give birth to piping phenomena causing partial or complete levee collapse during floods (Fishera et al., 2017). Earthen levee failures and collapses (a worst possible scenario) are linked also to other specific geological problems, in addition to those previously described. The main ones are synthetically listed below (but not discussed in detail in the paper been out of the goals of the work itself): inadequate thickness of the peat layer underlying the levee, over-topping, slope failure, seepage through the soils under the levee or seepage through the levees with pathways such as fractures/holes caused by natural processes, vegetation, human, and animal activities, and seismic shaking and collapse.

* Corresponding author.
E-mail address: veronica.pazzi@unifi.it (V. Pazzi).

https://doi.org/10.1016/j.jappgeo.2021.104376

A levee characterisation and monitoring system, that effectively recognises eventual problems before a disaster occurrence, has to inspect both shallow and deep areas of the structure and has to take into account both direct and indirect investigations, i.e., point and areal, respectively (Borgatti et al., 2017). In fact, at shallow depths, the detection will focus on leaks and voids, as well as normal degradation, disturbed material, and loose sandy material, while deep probing, throughout the levee thickness itself, will be sensitive to the levee material conditions (e.g., saturated areas, voids, loose materials) (Fishera et al., 2017). In literature Electrical Resistivity Tomography (ERT) and Ground Penetrating Radar (GPR) are the most employed geophysical techniques for a) imaging the levee internal structure, b) providing depthwise information about lateral variations, and c) delimiting high permeability pathways (Cho and Yeom, 2007; Niederleithinger et al., 2012; Cardarelli et al., 2014; Ikard et al., 2015; Busato et al., 2016; Bièvre et al., 2018; Allroggen et al., 2019). Levees general condition and strength as well as small changes to the interior of the tailing dam wall can be determined using seismic methods and seismic noise, respectively (Planès et al., 2016; Fishera et al., 2017; Olivier et al., 2017). Finally, ongoing seepage can be identified by means of self-potential surveys (Panthulu et al., 2001; Wilt and Corwin, 2005; Moore et al., 2011; Ikard et al., 2012; Rittgers et al., 2015).

Among the problems at shallow depth, animal burrows (erosion tunnels that enlarge the structure macro-porosity) severely compromise the integrity of the levees during a flood, in particular because of their often extensive and interconnected networks (Orlandini et al., 2015). Currently, the state of the art comprises case studies that deal with management and maintenance issues, while there are very few documented attempts at quantitatively assessing the damage caused by biological intrusions in an earthen structure, i.e., quantify possible animal-induced failure mechanisms (Bayoumi and Meguid, 2011; Orlandini et al., 2015). Both ERT and GPR are usually employed to detect voids in earthen levees that are generally placed at no more than a few metres depth (Chlaib et al., 2014; Busato et al., 2016; Borgatti et al., 2017; Bièvre et al., 2018). The spatial distribution of the underground electrical resistivities and the subsoil electric and magnetic properties changes can provide useful information to characterize subsoil anomalies of both natural and artificial (animal or human) origin (Santarato et al., 2011; Chlaib et al., 2014; Pazzi et al., 2016; Bièvre et al., 2018; Lai et al., 2018; Pazzi et al., 2018a; Pazzi et al., 2018b). Animal burrows usually behave as air filled caves and appear, therefore, as high resistivity zones with a different dielectric constant in contrast with the surrounding even relatively dry levee materials.

GPR techniques are based on the transmission, by means of an antenna, of electromagnetic (EM) waves into the soil and on the detection, by means of another antenna, usually located within the transmitter housing itself, of the echoes generated by the material property changes that affect the EM wave velocity, the attenuation, the polarization changes and redirection (Chlaib et al., 2014; Lai et al., 2018). Typically, GPR signals are pulses with a broad range of frequencies (10–5000 MHz range) that have different penetration depths. GPR is a non invasive high resolution technique characterized by a rapid data acquisition capability (Allroggen et al., 2019). Unfortunately, it is not really suitable for a 4D (over the time) monitoring.

ERT measurements, on the other hand, can be repeated to provide information on the evolution of resistivity with time (Bièvre et al., 2018). ERT in fact, is one of the most employed non invasive geophysical technique that allows to obtain the true ground resistivity distribution from measurements of currents (set by the operator) and voltages (induced in the soil by the generated current). These measurements, are usually performed with four electrodes in a quadripole configuration (Dahlin and Zhou, 2004; Santarato et al., 2011; Cardarelli et al., 2014; Busato et al., 2016; Pazzi et al., 2016; Morelli et al., 2020). The choice of the employed array configuration is a key point (Dahlin and Zhou, 2004), since each array has a different penetration depth and sensitivity (vertical/lateral resolution).

Between 2017 and 2018 a collaboration among physicists, geologists, and geophysicists of the University of Florence and of the National Institute of Nuclear Physics (INFN) Unit of Florence, has for the first time probed the possibility of exploiting the Muon Transmission Radiography (MTR) technique for verifying the internal conservation status of levees visibly damaged by animal activities (test sites are described in section 2.1). This new survey methodology and its application to the earthen levees are illustrated in section 2.2 and 2.3, while in Section 3 are presented the results of the field surveys. Finally, in Section 4 a discussion about the comparison and validation of the MTR data by means of 2D- and 3D-ERT measurements and the actual burrows' distribution mapped during the demolition works using Terrestrial Laser Scanner (TLS) measurements is provided.

2. Methodology and instrumentation

2.1. Test study sites

Two different areas in the Tuscany region of Italy were identified and selected as test sites, thanks to the support of the local authorities, of the companies responsible for the water supply system, and the existence of construction databases (e.g., Morelli et al., 2012): the South riverbank of the Arno River within the perimeter of the municipal aqueduct in Mantignano (Florence, Fig. 1 on left) and the North riverbank of the Bure stream in Pontenuovo (Pistoia, Fig. 1 on right). Both these sites were affected by the presence, on the levee flanks, of animal burrows entrance holes, as visible in Fig. 1, that strongly compromised the levee stability, and were therefore scheduled for restoration works that were subsequently performed after our measurement campaigns. These burrows entrance holes had diameters ranging from 0.5 m to 1.0 m. At the Mantignano test site the top of the levee was 3.0 m wide, with the South flank and the North flank having a slope of 33° and 30°, respectively and a height of 3.8 m. At the Bure test site the top of the levee was 11.0 m wide, with the North-East flank and the South-West flank having a slope of 40° and 30°, respectively and a height of 2.2 m and 4.2 m, respectively. Both levees were constructed with a uniform material (a mixture of sand, clay, and very fine gravels), with the absence of a low permeability core.

2.2. Muon radiography and muon tomography

Muon transmission radiography (MTR) and multiple scattering muon tomography (MSMT) are two slightly different muography techniques, that constitute a non-invasive survey methodology exploiting the space born corpuscular radiation continuously hitting the Earth's crust. These rays are mainly composed of muons, elementary particles similar to electrons but with a mass 200 times larger. Muons are produced in the top layers of the atmosphere by the interaction with the atmospheric gas of the isotropic flux of high energy particles, like protons, atomic nuclei, and less abundant species, which are commonly referred to as cosmic rays (PDG cap. 30, 2020). While most of the secondary particles produced by cosmic rays in the atmosphere are slowed down and absorbed by the atmosphere, muons are an extremely penetrating component that not only is present at sea level, but is capable of penetrating deep into the Earth's crust for up to hundreds of meters, depending on their energy. While traveling through materials muon trajectories are continuously modified by very tiny amounts, because of random electromagnetic interactions with the positively charged nuclei, thus determining a possible non-negligible overall deflection of these particles from their original trajectories (PDG cap. 34, 2020). The intensity of this effect, known as Multiple Coulomb Scattering (PDG cap. 34, 2020), is higher for low energy particles and increases with the atomic number Z of the traversed medium. The measurement of the deflection of muon trajectories upstream and downstream the volume of interest, is exploited in the MSMT technique to derive the 3D material distribution inside the volume under investigation (Bonechi et al., 2020b). If

Fig. 1. Test sites. Left: the Mantignano test site (red rectangle in the panel in the upper corner), the levee profile along the AA' section, and an upstream perspective photo of the levee. T1 is at the entrances of an animal burrow (shown in detail at the centre). Right: the Pontenuovo test site (red rectangle in the panel in the upper corner), the levee profile along the AA' section, and an upstream perspective photo of the levee. T2 is at the entrances of animals' burrows (shown in detail at the centre). At the centre, the location of the two test sites in Italy (upper) and a photos related to the T1 and T2 animal burrows entrances (bottom). The yellow cables employed to connect the ERT electrodes at both test sites are visible in the pictures (lower left and right corners). (For interpretation of the references to colour in this figure legend, the reader is referred to the web version of this article.)

the traversed thickness is sufficiently large, the lowest energy muons can be definitively stopped, finally decaying into electrons, quickly absorbed inside the material, and neutrinos, which instead move away undisturbed. The consequent reduction of the muon flux intensity is the effect which is used in the MTR technique to provide information on the density distribution inside the material volume under investigation.

For large target volumes, like volcanoes, mining sites, dams, or river levees, MTR is the only practically usable muographic technique and it is implemented by counting the number of muons that traverse the structure in front of the detector. Muon track angular distributions are measured only downstream of the volume of interest and later compared with similar measurements performed looking at a free portion of the sky, with the detector pointing in the same direction, in such a way as to allow an estimation of the directional muon transmission, defined as the fraction of muons that survives for each direction after traversing the target. More details concerning the muographic methodology can be found in literature (Bonechi et al., 2020b).

If θ and ϕ are the zenith and azimuth angles representing a particular direction, the muon flux measured by a detector from a solid angle $d\Omega$ around that direction will be given by the following equation:

$$\Phi(\theta,\phi) = \frac{\Delta N(\theta,\phi)}{d\Omega \cdot \in \cdot S(\theta,\phi) \cdot \Delta T} \tag{1}$$

where $\Delta N(\theta,\phi)$ is the number of muons collected in the solid angle $d\Omega$, $\in$ is the detector global efficiency, $S(\theta,\phi)$ is the effective surface of the detector for the direction (θ,ϕ) and ΔT the live time of the acquisition.

Therefore, it is possible to define the transmission (or transparency) $t(\theta,\phi)$ as the target (T) over the free sky (FS) ratio of the measured muon flux obtaining:

$$t(\theta,\phi) = \frac{\Phi_T(\theta,\phi)}{\Phi_{FS}(\theta,\phi)} = \frac{\Delta N_T}{\Delta N_{FS}} \frac{\Delta T_{FS}}{\Delta T_T} \frac{\in_{FS}}{\in_T} \frac{S_{FS}}{S_T} \tag{2}$$

where the direction dependencies have been omitted in the last expression for clarity and the subscripts refer to the configuration under consideration. The ratio of the efficiencies, in normal operating conditions, will be approximately equal to one while the ratio of the effective surfaces will be exactly equal to one if the pointing direction of the detector remains unchanged between the two configurations (free sky and target).

The MTR technique can be exploited comparing the measured 2D angular muon transmission distribution, defined in (2), with a simulated distribution including all the available information on the expected muon flux, the geometry of the target volume and the constituent materials. A 2D distribution of the measured/simulated transmission ratio gives directional information on potential deviations of the measured muon flux from the expected one, thus suggesting angular regions where the available information does not describe satisfactorily the real structure of the target volume.

Section 2.3 gives a more detailed description of the methodology used for this work. The field surveys results are reported in Section 3.

2.3. Application of muon transmission radiography in the identification of cavities within river levees

The measurements described in this paper have been achieved using MTR, i.e., determining the fraction of muons that are able to completely pass through the material volume under examination. Because of the angular dependence of the atmospheric muon flux, which is maximum in the vertical direction and decreases approximately as the square of the cosine of the zenith angle, the detector has to be installed as far

below as possible to the volume under observation. In the particular application described in this paper the detector could not be installed much lower than the target. The instrumentation was placed at the foot of the levee and consequently, the detection of muons at elevations lower than 10° − 20° (i.e., traveling almost horizontally, in an angular region where the flux intensity is very low and the average muon energy high) was required.

As stated before, because of the high penetration capability of the muon projectiles the muographic technique is quite capable of probing rock layers with a thickness of tens of metres. In the case of earthen river levees, the typical structures spans thicknesses ranging from a few metres to ten-twenty metres, with a height of a few metres, with highly compacted soil volumes, whose density is usually not very large (below 2 g cm^{-3}). The material thickness seen from the detector point of view is typically of the order of few meters and the muon absorption effect is consequently small. These characteristics, make the study of riverbanks a demanding case in the application of muographic techniques since most of the quasi-horizontal muons will anyway survive passage through the levee thus washing out the signal that comes from the absorption. Nonetheless, enough data (and statistics) have been acquired to obtain some interesting results that will be discussed in the next sections.

For the muographic studies presented in this work, the MIMA (Muon Imaging for Mining and Archaeology) charged particle tracker has been employed. MIMA is a rugged and compact prototype detector, expressly designed to allow its installation in inhospitable environments like mining, archaeological structures, and inside dams, but it was never used to study volcanoes given its relatively small size (Baccani et al., 2018; Bonechi et al., 2020a). The muon detection relies on the scintillation effect produced by the passage of charged particles through specific materials, called scintillators. In particular MIMA is composed of three pairs of detection planes made with 40 cm long bars of high quality plastic scintillator. Each pair of planes allows the measuring of the two (x,y) coordinates of the muon impact points along its trajectory. The measurement of three impact points for each muon allows the unambiguous reconstruction of the muon trajectories, avoiding possible random coincidences due to muon showers or electrical noise. The tiny light signals produced inside the scintillator bars are converted to electric signals and amplified using silicon photomultipliers (SiPM), optical sensors positioned at the two ends of each bar and glued to the scintillator with optical adhesive.

Six custom front-end electronic boards derived from the MURAVES experiment (D'Errico et al., 2020), based on the EASIROC chip, are used for the amplification and digitization of signals coming from the 21 output lines from each detector plane. An independent digital acquisition board, controlled by a miniaturized Raspberry PI computer, houses an FPGA implementing the selection criteria of events to be registered and takes care of collecting the output data streams from all the front-end boards, which are finally saved to a 64 GB SD card installed on board the Raspberry PI computer. The detector modules are assembled inside a thin aluminum box and fixed on an altazimuthal mechanical mounting which allows changing the detector's pointing direction with an accuracy of approximately one degree.

The spatial resolution of the MIMA tracking planes has been measured using muon tracks acquired at free sky and obtaining a value of 1.6 mm for the single final plane installed in MIMA. The resulting angular resolution, considering the geometrical design of the detector, is approximately 6.7 mrad. The linear uncertainty for detecting a target 10 m far away from the detector (typical distance in the application presented in this paper) is approximately 6–7 cm, which is quite smaller than the expected size of the holes to be detected. Better angular resolution could help getting more defined images, but a sort of limit to image definition is due to the deflection of muon trajectories caused by multiple collisions with molecules happening while crossing the riverbank structure. The currently adopted configuration represents a compromise to have a precise tracker at an affordable cost. Further details on the detector and its performance can be found on (Bonechi et al., 2020a).

2.4. Muographic apparatus placement and measurements

A first test using MTR was planned just after the first assembling of the MIMA detector starting in the middle of 2017. This activity, that allowed among the other things testing the detector's transportation and installation procedures, was carried out in a protected area with the advantage of having a safe installation point and the availability of the power mains (see Fig. 1 on left).

MIMA was first installed at the Mantignano site, in front of the levee, 4 m far from its external foot. A 50 cm deep hole in the ground was dug so as to install the detector as low as possible with respect to the region to be studied. The detector's pointing direction was fixed at approximately 3° azimuth (magnetic north) and 14.7° elevation corresponding roughly to the direction of the top of the levee as seen from the detector's installation point. The data acquisition in the target mode configuration lasted 8 days only, because longer data taking in front of the levee body was not possible due to the scheduled demolition and reconstruction of the levee structure. Therefore, given the small detector's acceptance, only a small data set was collected. During the excavation work carried out to restore the levee it was not possible to verify the actual extension of the cavities seen by MTR inside the soil. The free sky measurement was carried out from the second floor of an aqueduct building placed near the levee. A planar distance even of some tens of kilometres and few tens of meters in altitude would not have appreciable effects on the muon flux. In case of sensibly different latitudes, corresponding to distances of hundreds of kilometres on the ground, or a difference of some hundreds of meters in altitude could affect the measure and should be taken into account for reliable comparisons. The acquisition duration was of about 7 days in this free sky configuration, and the detector efficiency remained stable during the two measurements.

Following the experience at the Arno River levee in Mantignano a new measurement was proposed at the Bure Creek levee in Pontenuovo near Pistoia, where a long stretch of the levee had been badly damaged by animals. The purpose of this new campaign was to obtain a more detailed comparison of the muographic and the geoelectric techniques and to verify the results with direct measurements of the animal burrows during the scheduled levee demolition. In Fig. 2 a picture referring to the instruments installation (the TLS on front, the MIMA detector in the middle, and on the back the yellow cables employed for the ERT acquisition) in the Pontenuovo area is shown.

The survey at the Pontenuovo test site was carried out between June and August 2018. The installed apparatus was almost the same as in the previous case, but the location identified for the installation was inside a private field where the power mains was not available. A powering system composed of four photo-voltaic panels, a charge controller and a battery, capable of maintaining the whole system alive 24/7 was installed, with the electronics placed in the same protection box containing the MIMA detector. Also in this case, the detector was pointed towards the top of the bank body perpendicularly to the levee axis itself corresponding to an elevation of approximately 16° and an azimuth of −149.7°. The acquisition time for the target configuration was of about 23 days while the free-sky data were collected for 21 days, after moving the detector to the top of the levee. The efficiency of the detector remained unchanged between the two acquisitions.

The maps of the reconstructed tracks distribution in the target configuration $N_T(\theta,\phi)$ for the two sites are illustrated in Fig. 3. The plots show the angular distributions of the detected muons with a two-dimensional representation, where the direction of motion of the muons is identified by the azimuth (x-axis) and elevation (y-axis) angles of their tracks. The same choice has been made also for the other angular maps reported in this paper. On both axes a 2° bin size has been chosen. The characteristic shape of the resulting images appearing in these plots is determined by the detector acceptance, which was

Fig. 2. Installation of MIMA (within the wooden box) in front of the levee body at the Bure creek. In this photo are also visible the TLS, on the front, and the ERT yellow cables, on the back. (For interpretation of the references to colour in this figure legend, the reader is referred to the web version of this article.)

slightly different for the two setups. At the time of the Mantignano measurement only tracks hitting all of the six planes of the detector were selected to avoid, as previously stated, reconstructing fake tracks using random hits appearing on two pairs of planes. Because the analysis of triggered events showed that the number of such kind of events is negligible, for the Bure site the acceptance was increased by selecting all tracks crossing at least four of the six tracking planes. A cross check was anyway performed to verify that no spurious events contaminated the data sample. The maximum density of the detected muon tracks is observed at an intermediate interval of the elevation between the vertical direction, where the muon flux is maximum, and the detector's pointing direction, at which the detector's acceptance is maximum. The muon absorption effect due to the presence of the levee body is not visible at this stage, due to the relatively small thickness of the levee body.

For both surveys the region under investigation is in a range of elevations between approximately 6° and 15°. At the Pontenuovo test site, given the duration of the data taking, the number of muon events in each bin is of the order of a few hundred, which translates in a statistical uncertainty of the order of a few percent for each bin. For the Mantignano measurement, with an acquisition time reduced to a third, the number of detected muons per bin is less than one hundred, with a corresponding decrease of the statistical precision.

2.5. ERTs layout and measurements

In order to achieve the measurement campaign goals (i.e., identification of the subsoil distribution of the animal burrows and comparison with the results of the MTR survey), 2D- and 3D-ERTs were planned and carried out at the two test sites (Fig. 4). In fact the 3D-ERT acquisition, collects soil resistivity data both behind the electrodes and in the surrounding volume (Pazzi et al., 2018a). The electrodes' arrangements were chosen so that the ERT section length would correspond (1 m larger) to the maximum angular view of the MIMA detector. In particular, at the Mantignano test site a 3D-grid layout survey (24E x 3 L: 24 electrodes (E) along 3 lines (L), green dots in the left panel of Fig. 4) and a 2D profile (red dashed line in the left panel of Fig. 4) coinciding with the inner line of the 3D survey were carried out. At the Bure site, instead, two 3D surveys with different electrodes arrangement were performed: a 3D-loop/rectangular layout

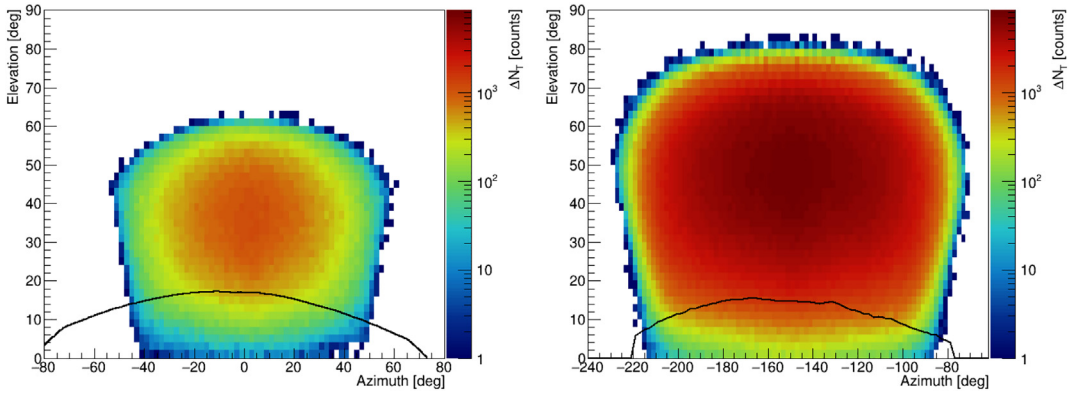

Fig. 3. Muon angular distributions for the target configuration at Mantignano (left) and at Pontenuovo (right). The black line shows the levee profile as seen from the detector point of view (the visual effect is similar to that shown at the bottom of Fig. 7).

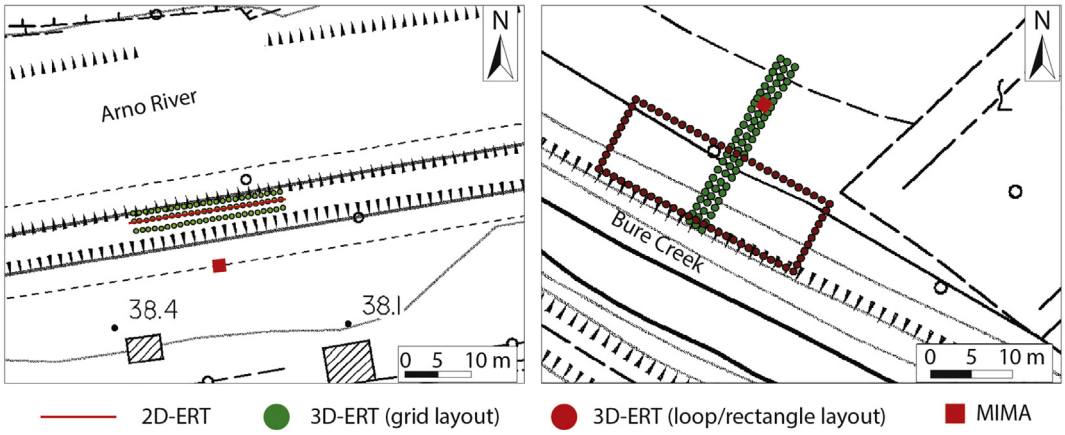

Fig. 4. The ERTs survey layouts on a topographical map freely available from the Tuscany Region administration (https://www.regione.toscana.it/-/geoscopio). Left: the survey performed at the Mantignano test site (green dots represent the 3D survey, while the red line represents the 2D one). Right: the survey performed at the Pontenuovo test site (green and red dots represent the two different 3D surveys). In both panels the red square (not in scale) is MIMA. (For interpretation of the references to colour in this figure legend, the reader is referred to the web version of this article.)

survey (26 × 11 electrodes, red dots in the right panel of f Fig. 4) over the levee's top and a 3D-grid layout survey (24E x 3 L, green dots in the right panel of Fig. 4) over the levee's top and the North-Eastern flank around a large tree (visible over T2 in Fig. 1). All the 3D-ERTs were acquired by means of 72 electrodes through a 24-electrode external link connected to the Iris SyscalPro 48 electrodes (10-channels receiver). Stainless-steel stakes were used as electrodes and the fixed distance between two adjacent electrodes was set equal to 1 m.

All the layouts were acquired with the dipole-dipole (DD) and the pole-dipole (PD) arrays since they are more sensitive to lateral electrical resistivity variations, have enhanced lateral resolutions at shallow depths, are subject to minimal electromagnetic inductive noise, and combine consistent signal strength with a high resolution and large depth of investigation (Loke and Barker, 1996; Dahlin and Zhou, 2004; Szalai and Szarka, 2008; Santarato et al., 2011; Pazzi et al., 2018a; Pazzi et al., 2018b; Pazzi et al., 2020). At the Mantignano site the 2D-ERT PD acquisitions were collected using two different remote poles placed on the levee top (one 100 m far from the profile along the East direction, and the other at the same distance along the West direction). The measurements were then all inverted simultaneously to reduce the effects of remote poles finite location. The remote pole of the 3D-ERT, instead, given the longer acquisition time, was placed as far away as possible along the South direction starting from the middle of the 3D-grid. At the Bure test site one remote pole for both 3D layouts was placed as far as possible along the North direction. The acquisition sequences were planned to take advantage of the multichannel instrument system (Santarato et al., 2011) and in total at the Mantignano and Bure sites 12,093 (2D: 2456, 3D: 9637) and 16,940 (3D-grid: 6861, 3D-loop: 10079) apparent resistivity values were acquired, respectively. All the measurements were carried out in the July–August dry season.

All the electrodes were geo-referred by means of a differential GPS in Real Time Kinematic mode, and a detailed Terrestrial Laser Scanning (TLS) of the surrounding area was performed to optimise the inversion procedure (Pazzi et al., 2020). The TLS measurements were carried out using a Riegl VZ-1000. The apparent resistivity data inversion was performed using the commercial software ErtLab© (developed by Geostudi Astier S.r.l.) that employs a finite element method and divides the subsoil model into triangular cells (Santarato et al., 2011; Viero et al., 2015; Pazzi et al., 2018a; Pazzi et al., 2020). For each site, the apparent resistivity value of the starting homogeneous half-space was chosen equal to the mean apparent resistivity value of the whole dataset. Even if levees crests are considered as flat structures, 3D topographic effects have to be taken into account anyway (Bièvre et al., 2018). The selected software is able to manage these topographic effects (Santarato et al., 2011; Pazzi et al., 2020).

3. Results

3.1. ERT results at the Mantignano and Pontenuovo sites

The ERTs surveys were carried out during two working-days, one for each site. Given the dry condition of the soil during the field surveys, some of the acquired apparent resistivity data resulted having a high standard deviation value (acceptable values were set equal to 2%) and were therefore removed before the inversion process. The total amount of removed data, for both the test sites, was equal to roughly 20% of the whole acquired data. The employed inversion software implements a finest data noise management, using Occam's regularization, and allows to set different percentage values of the standard deviation noise (noise in the following), according to the quality of the dataset (see Pazzi et al., 2020 and references within for a detailed discussion). By default these values were set equal to 5. The quality of an inversion is calculated minimizing the misfit function between the field and modelled data and can be summarized with the number of iterations need to reach the process convergence (Santarato et al., 2011; Pazzi et al., 2018a). If the number of iterations is too low (3 or less) it is recommended to reduce the noise. On the contrary, if the process does not reach the convergence after a maximum number of iterations set by the operator (usually between 10 and 20) the noise has to be increased. All the ERTs inversions were carried out with noise values equal to 2. The convergence at the Mantignano and Pontenuovo sites was reached, for all the layouts, after 7 and 8 iterations, respectively.

The results of the 2D- and 3D-ERTs obtained from inversion at both test sites of all the acquired data, are shown in Fig. 5. The levees are characterized by uniform resistive values (up to 200 Ωm, blue colour) typical of a dry mixture of sandy clay and very fine gravel soils. At the Mantignano site (left in Fig. 5) the high resistive anomalies (in the range of 300–600 Ωm associated with green to yellow colours) within the levee body and highlighted with a black dashed line can be associated to holes filled with air. At the Pontenuovo site (right in Fig. 5) empty cavities are marked as orange volumes (resistivity values higher than 900 Ωm). Moreover, here the resistive anomaly highlighted by the black arrow is caused by a combination of various animal burrows and the invasive tree roots (both visible in Fig. 1) that have similar resistivity ranges.

3.2. MTR results at the Mantignano and Pontenuovo sites

In muon radiographies the quantity that is usually reported is the directional muon transmission, i.e., the fraction of muons that survive after traversing a volume of material along a particular direction. An angular distribution of this quantity as seen from the detector's center can

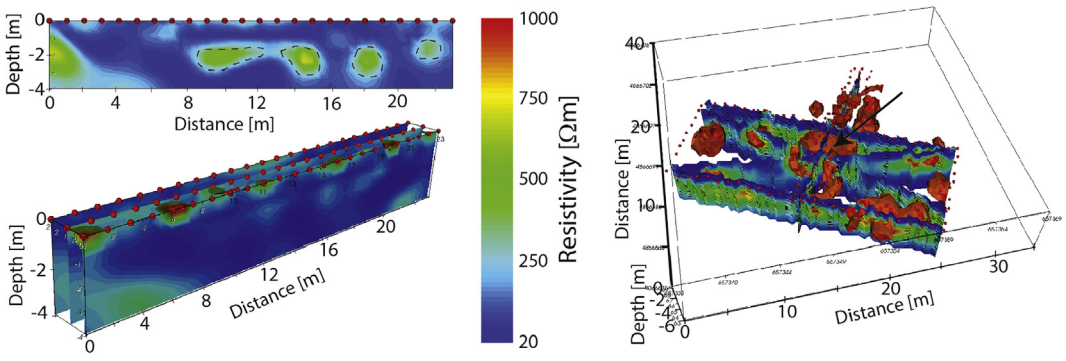

Fig. 5. ERTs results. Left: 2D and 3D ERTs at the Mantignano site. The black dashed line highlight anomalies caused by the animal burrows. Right: 3D ERT results at Pontenuovo site. Orange volumes are the animal burrows, while the black arrow indicates a resistive anomaly caused by the combined effects of animal burrows and tree roots.

be obtained by calculating the ratio of the measured target and free sky angular distribution of muons evaluated as described by eq. 2 at the end of Section 2.2. In the left plot of Fig. 6 the measured angular map of muon transmission at the Mantignano site is shown. Blue regions are those for which the transmission is larger (above 95%), while the transmission decreases approximately to 90 % − 92% in the brown regions. The profile of the levee body appearing in this plot, though not sharp, is in optimal accordance with the black line obtained from the embankment topography. A smoothing algorithm has been applied to reduce statistical fluctuations. The right plot in Fig. 6 is an enlargement of the central portion of the region of the studied levee just in front of the detector, where two holes dug by animals were visible on the opposite side (internal slope), 5 m far from each other. On the same plot some indications of the linear size of the observed anomalies are reported, obtained by projecting the angular information at a distance of 12 m (corresponding to the distance of the levee median plane). The total extension of the anomalous region in this hypothesis is of the order of 5 m as expected from the previous visual inspection.

The simulated muon transmission and the measured-to-simulated transmission ratio (also known as relative transmission) are reported in the supplementary material (see Fig. S1). From the relative transmission map the high transmission signals below the levee profile are still visible while the sky-embankment transition, visible in the measured transmission map, is now removed. As previously stated, the demolition and subsequent reconstruction of the levee body was done right after the MTR measurement but an identification of the real burrows distribution was not performed because of logistic problems.

The angular distribution of the muon transmission at the Pontenuovo site is shown in Fig. 7 top left. The measured transmission map shows several interesting characteristics. First of all a separation between the free sky and the levee can easily be identified, which is in agreement with the topographical profile of the levee, shown as a continuous line at an elevation of roughly 15° in front of the detector. For azimuth values around −130° a clear shadow is found. This is due to a big tree located near the top of the levee body, as shown in the bottom picture of Fig. 7. Focusing the attention to the region below the expected profile of the levee, some zones with high measured transmission can be found, which can be interpreted as empty cavities and tunnels developing inside the structure.

The simulated transmission is reported on the top right of Fig. 7 with the same angular range and colour scale used for the measured transmission map. The simulation was obtained considering a uniform undamaged levee made of soil with density of $d = 1.8 g/cm^3$. The embankment topography was detected through TLS surveys but the trees and the burrows were excluded from the simulation since the latter were the object of the studies. The anomalies in the measured transparency caused by the tree and the tunnels inside the bank are highlighted by looking at the relative transparency map reported in Fig. 8. In particular the tree appears as a region of low relative transparency while the high signal regions below the embankment profile could be associated with low density volumes (such as tunnels dug inside the body structure).

4. Discussion and future perspectives

In this study, the results of the first application of the MTR technique to study animal burrows within earth levees are presented. To understand the potential of this technique, ERTs and TLS measurements,

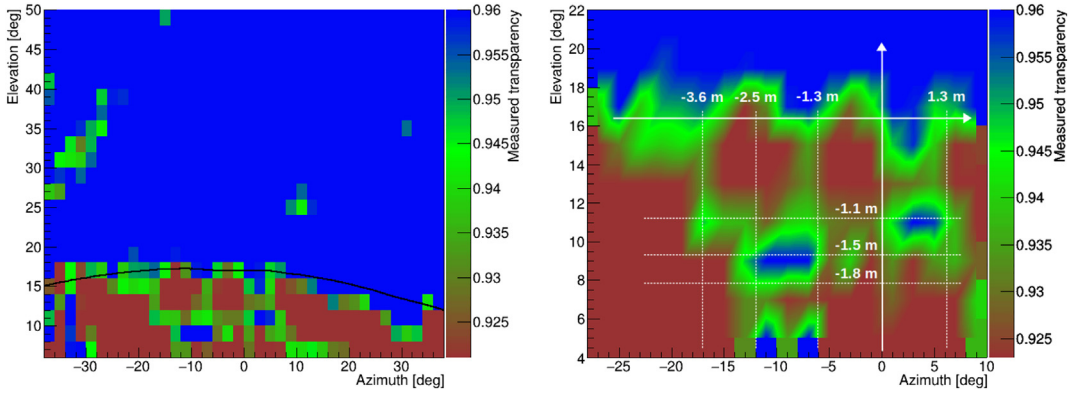

Fig. 6. Left: measured angular distribution of muon transmission through the levee body of the Arno river in Mantignano. The black line denotes the levee profile as seen from the detector point of view and the absorption effect due to the levee structure is clearly visible below this line. Right: zoom in of the angular region in front of the detector, where two den entrances, 5 m far from each other, were visible. On the same map a linear grid is obtained projecting the angular dimensions at a distance of 12 m (which is the distance of the levee median plane).

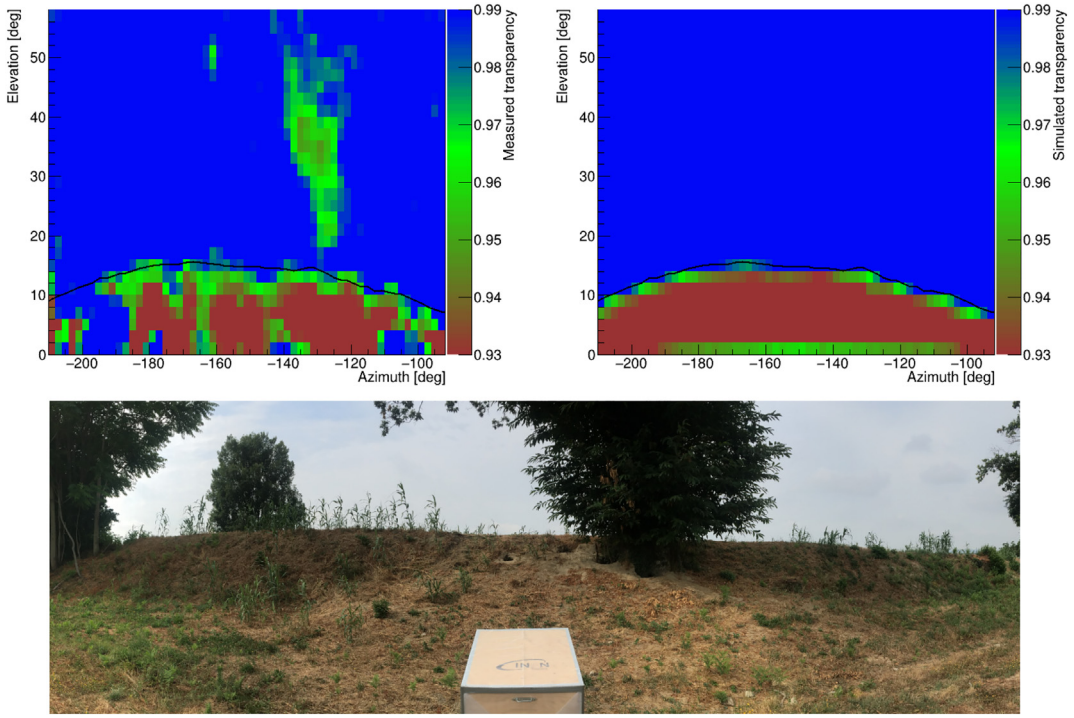

Fig. 7. Top: angular distribution of muon measured transmission (left) and uniform levee simulated transmission (right) from the detector's installation point at the Bure creek's levee in Pontenuovo (Pistoia). The black line denotes the embankment profile as seen from the detector point of view. Bottom: picture of the levee and of the tree as seen from the detector. It is possible to observe the correspondence between the measured transmission and the photo of the measurement setup.

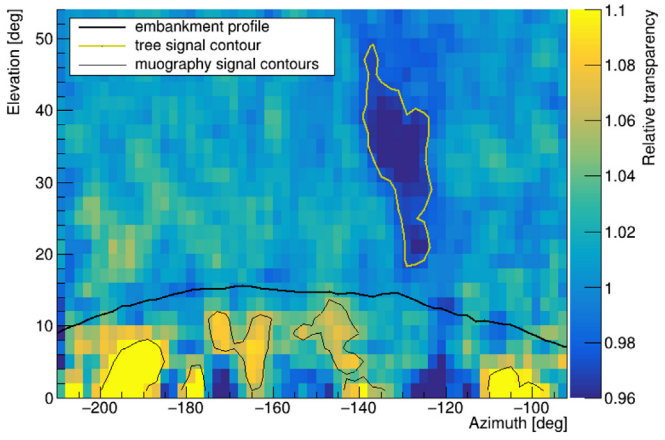

Fig. 8. Angular distribution of muon relative transmission (measured-to-simulated transmission ratio). The embankment profile is shown only as a reference: if anomalies were to be absent, no variations would be expected below the line.

two more traditional and commonly used methods in this field, have been carried out. It is important to underline that the MTR applied to study the inner levee works borderline the application limits of the technique itself. The muon detector, in fact, works at an angle of only a few degrees above the horizon, where the muon flux is very weak (see Section 2.3). Moreover, in this type of application the average opacity of the target structure (product of thickness and average material density) is a little too low for the MTR technique and the animal burrows quite small to be easily identified; the only feature determining an increase in muon transmission is the size of the void along the detector line of sight. Nevertheless, also the transverse extension of the void is important. In case of a very narrow hole developing along the detector's line of sight (i.e., a burrow parallel to the trajectories of muons entering the detector), even if very long, it might be impossible to be detected because muon deflection in the surrounding material could result in a relevant smearing of the signal. The preliminary measurements carried out at the Mantignano site were fundamental to improve the hardware setup and all the procedures and to test the detector remote control, by continuously monitoring the detector itself with a network connection realized with a 3G modem. The measurement carried out at the second site (Pontenuovo) was instead instrumental in the understanding of the MTR technique potential and reliability.

As scheduled by the Bure levee restoration works, one month after our geophysical field survey, a trench (mainly 1.2 m wide except in correspondence of the tree, 30 m long, and 2.0 m deep; yellow dashed line in Fig. 9) was dug in correspondence of the centre line of the levee. This trench was completed in three different steps and allowed us to identify 27 cavities. Probably, the number of animal burrows could be higher still, especially in the central part of the analyzed volume, since during the second step of the excavation works a different technique was employed that allowed a more rapid advancement, but destroyed some cavities. The entrance of each cavity was mapped thanks to a TLS survey, that was performed also to acquire the levee topography, allowing to precisely locate the animal burrows within the levee body. The overall direction and depth of each cavity, on the contrary, was measured by means of a rigid pole. Therefore, it was not possible to precisely reconstruct the 3D geometry (e.g., as in Borgatti et al., 2017). In fact, the 3D development of each cavity was schematised using cylindrical volumes superimposed on the TLS map (Fig. 9).

Among all the detected cavities only those located in the same volumes surveyed by both ERT and MTR, were used for the comparison. The 3D distribution of the resistivity anomalies higher than 900 Ωm (light blue volumes in Fig. 9) and of the entrance of the detected animal burrows (coloured cylindrical volumes in Fig. 9) overlap quite extensively. In Fig. 9) two areas are shown as an example. The first one (marked with A) is in correspondence of the tree. Here, the high resistivity volume is generated by the combination of animal burrows and the tree roots (see also Fig. 5) that have similar resistivity ranges. The

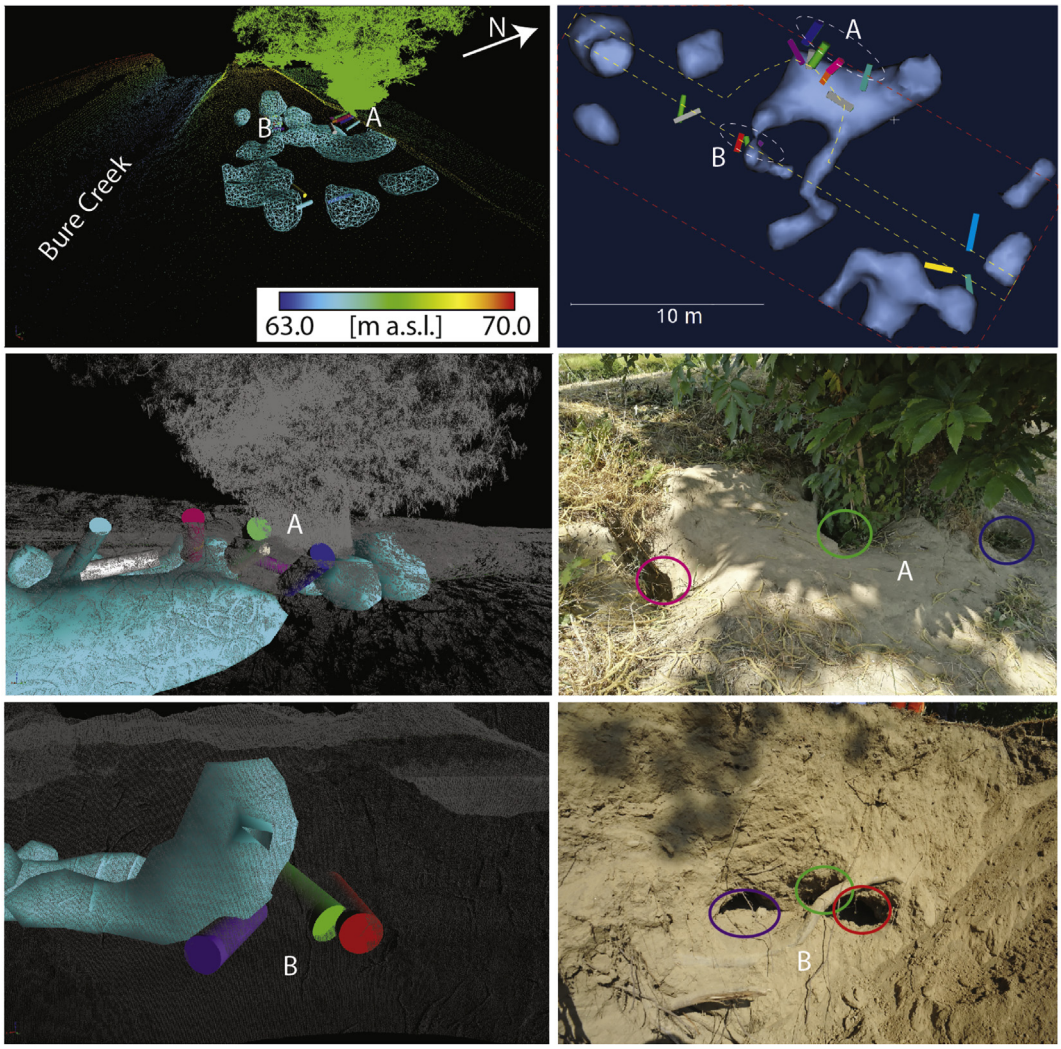

Fig. 9. Comparison between the ERTs results (in light blue) at the Pontenuovo site and the reconstruction as cylindrical volumes of the animal burrows. Top: in the left corner a 3D view from east of the levee, while in the right corner the view from South. In this panel the dashed red line marks the boundary of the 3D-ERT survey, while the dashed yellow one that of the trench. Centre: at left the 3D view from North-East of the ERT anomalies and of the animal burrows under the tree and marked with A, while at right a photo of the animal burrows entrance under the tree (the three coloured circles represent the bases of the cylinders). Bottom:left, the 3D view from North of the ERT anomalies and of the animal burrows in the middle of the levee marked with B, while at right a photo of the animal burrows entrance (the three coloured circles represent the bases of the cylinders). (For interpretation of the references to colour in this figure legend, the reader is referred to the web version of this article.)

second area (marked with B) is in correspondence of three holes detected during the trench excavation in the middle of the levee.

As already explained MTR, acquired using just one view angle, gives only a 2D information of the whole volume since it projects along the radial direction to the detector surface. Although in some cases it is possible to carry out a 3D reconstruction of the MTR signals, even with a single measurement (Bonechi et al., 2015), it is not possible to do so in this case due to the limited statistic of the acquired data. Therefore, a possible way to compare the muon radiography results with that of the other two techniques (ERT and TLS) is to build 3D projection cones. These cones starts from the contours of the signals shown in Fig. 8, with the cone apex placed at the center of the MIMA tracker. Using this method an excellent correspondence for the tree signal and the real position of the base of the tree itself was found, because it stands out against a background of air (see the movie uploaded as supplementary information). Since muon transmission is sensitive to the material density, it is important to underline that if roots and soil have similar densities, they appear similar to muon transmission radiography. Therefore, the average density in the corresponding angular regions might not be significantly different from the surrounding angular regions characterized by compact soil. Differently, voids appear as angular regions characterized by a lower average density.

Another possibility to compare results of different acquisition techniques is to refer the ERT and TLS surveys to the point of view of the detector, bringing their 3D information into the 2D muography maps. This method has the advantage of producing bi-dimensional images that are easier to study and interpret. In order to proceed, for both techniques, those volumes which are assumed to be composed of air have to be identified. In case of the TLS surveys the reconstructed cylinders corresponding to the identified burrows were selected, while for the ERT measurements those volumes with an inner resistivity higher than that of air were identified. Air resistivity can vary greatly from case to case and for this analysis at the Bure site a value of $\rho_{air} = 900\,\Omega\mathrm{m}$ was chosen. Given this minimum value, the corresponding isosurfaces are built using the CGAL library (The CGAL Project, 2020) and the result is reported in Fig. 9 as light blue volumes.

The thickness of the high resistivity volumes as seen from the muon detector position is shown on top of Fig. 10. For a given direction multiple volumes can overlap contributing to an increase of the overall thickness of the air volume. Since the air volume is greater for the ERT

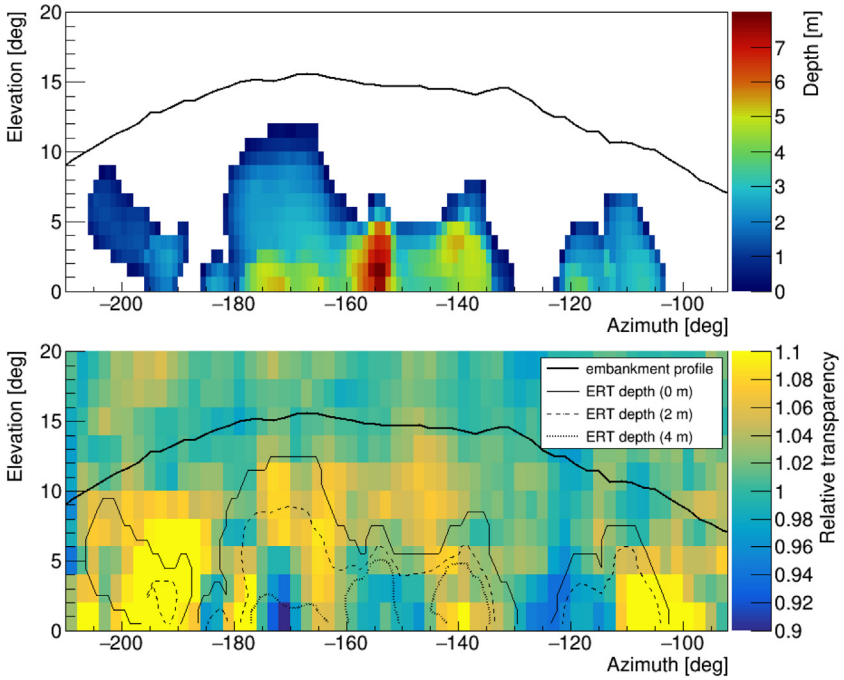

Fig. 10. Top: air depth maps from the MIMA point of view for the high resistivity volumes. Bottom: muon relative transmission map with the contour lines of the high resistivity volumes for various depths. Analogous plots are reported in the supporting material for the cylinders detected with the TLS.

volumes than for the TLS cylinders, the former will be more easily visible from the MTR. For completeness the air depth map associated with the TLS cylinders is reported in the supplementary material (see Fig. S2).

In order to superimpose the thickness of the high resistivity volumes on the relative transmission map obtained from the MTR measurements, the contour lines of the air depth map were drawn as shown on the bottom of Fig. 10. Comparing the MTR map with the air depth contour from the ERT surveys, it is possible to see that there is an optimum match in three regions (azimuth in the range $[-200°, -190°]$, $[-145°, -135°]$ and $[-120°, -100°]$) where the high signal in the relative transparency map corresponds to a large thickness of high resistivity volume. For azimuth values in the range $[-185°, -160°]$, although the agreement is not perfect, the regions with high relative transparency are still within the first contour line (outlined by the thin black line).

The results of the first application of the MTR technique here presented show its reliability in accurately characterizing the inner structure of an earthen levee. Nevertheless, some limitations have also been shown. First of all the muon detector dimensions are strictly related to the size of the object to be visualised: the smaller the detector, the smaller the levee portion that can be investigated. Secondly, since it is not possible to place the muon detector at a high angle over the horizon, the data acquisition time can be quite long (order of many weeks), in order to obtain a satisfactory statistics. Finally, to reconstruct the actual volumetric distribution of the burrows it would be better to acquire measurements of the same portion of the levee from different angles. These drawbacks can be solved by enlarging the muon detector dimensions, by trying to place the detector within a hole to increase the angle over the horizon, and by setting up more than one detector at the same time.

Moreover, this first application of MTR to characterize the inner part of the levees also shows some pros of the technique itself over the existing ones. For example, the MTR can be performed without removing the vegetation gowned up on the levee's top (as it appended in this study at the Bure site). Another advantage is that MTR is influenced only by the materials' density variations and not by other environmental conditions (e.g., the subsoil saturation). Thus, by means of the MTR is it possible to distinguish between voids and roots that, at the contrary, appear in the ERTs profiles as anomalies with the same resistivity ranges. Therefore, combining MTR and ERTs, voids can be identified as high resistivity anomalies with a high muon transparency, while roots as resistivity anomalies with a muon transparency equal or similar to that of the undisturbed levee. Moreover, since the subsoils saturation does not change significantly the soil density, compared to the voids one, it is possible to compare the results of MTR acquired with different saturation conditions and perform a time-lapse (4D – time dependent) analysis. Some additional studies are required to understand the benefits in the 3D anomalies reconstructions since also ERT and/or GPR techniques can provide this kind of information, as well as to evaluate the reliability of MTR as an earlier warning technique. Moreover, at this state of the research the MTR technique cannot be considered a resource capable of having a direct impact on the management of flood emergencies along all statistically predictable areas because of its analytical characteristics and physical constraints. However, in the near future, it could play a decisive role in the management of the hydro-geomorphological regime of a river in some key points. For example, MTR could be successfully applied to characterize the structural integrity of dams since the instruments can be placed both within the dam itself, in the inspection gallery/ies (an application has been carried out by our team, but results are not jet published), and facing the downstream slope. In both cases the measurements can be carried out avoiding the draw-down of the backwater. An early diagnosis of any criticality (and therefore timely intervention), in fact, is here considered essential to avoid consequences on the ordinary river dynamics and especially the flood control.

5. Conclusions

This study shows the potentialities and the reliability of the MTR technique in the characterisation of earthen levees inner structures. Although this application is at the limits of the technique itself (for zenith angles larger than 90° the muon flux is practically null), the comparison between the ERTs and MTRs maps shows that the MTR is a suitable and promising technique that could successfully complement a program of geological risk assessment. The MTR maps, in fact, show high transparency values in correspondence of the animal burrows. This first application also highlighted some limitations like:

a) the small detector dimensions, b) the long time of acquisition, and c) the need of employing more than one detector to obtain a reliable 3D reconstruction.

CRediT authorship contribution statement

G. Baccani: Conceptualization, Methodology, Software, Validation, Formal analysis, Investigation, Resources, Data curation, Writing - original draft, Writing - review & editing, Visualization. **L. Bonechi**: Conceptualization, Methodology, Software, Validation, Formal analysis, Investigation, Resources, Data curation, Writing - original draft, Writing - review & editing, Visualization, Supervision, Project administration, Funding acquisition. **M. Bongi**: Software, Validation, Formal analysis, Writing - review & editing. **N. Casagli**: Supervision, Funding acquisition. **R. Ciaranfi**: Software, Validation, Formal analysis, Writing - review & editing. **V. Ciulli**: Conceptualization, Methodology, Formal analysis, Investigation, Writing - review & editing, Supervision. **R. D'Alessandro**: Conceptualization, Methodology, Investigation, Writing - review & editing, Supervision, Project administration, Funding acquisition. **S. Gonzi**: Software, Validation, Formal analysis, Writing - review & editing. **L. Lombardi**: Conceptualization, Methodology, Validation, Formal analysis, Investigation, Resources, Data curation, Writing - review & editing, Visualization, Supervision, Project administration. **S. Morelli**: Conceptualization, Methodology, Investigation, Writing - review & editing. **M. Nocentini**: Conceptualization, Methodology, Investigation, Resources, Writing - review & editing. **V. Pazzi**: Conceptualization, Methodology, Validation, Formal analysis, Investigation, Resources, Data curation, Writing - original draft, Writing - review & editing, Visualization, Supervision, Project administration. **C. Tacconi Stefanelli**: Conceptualization, Methodology, Investigation, Writing - review & editing. **L. Viliani**: Software, Validation, Formal analysis, Writing - review & editing.

Declaration of Competing Interest

The authors declare that they have no known competing financial interests or personal relationships that could have appeared to influence the work reported in this paper.

Acknowledgement

Authors want to thank the public institution Regione Toscana, the local authorities of Florence and Pistoia in charge of the maintenance of the levees, Publiacqua S.p.a. (the company responsible for managing the public water distribution), and the Consorzio di Bonifica 3 Medio Valdarno (the institution responsible for safeguarding the territory from geo-hydrological risk) to allow them performing the measurements.

Appendix A. Supplementary data

Supplementary data to this article can be found online at https://doi.org/10.1016/j.jappgeo.2021.104376.

References

Allroggen, N., et al., 2019. High-resolution imaging and monitoring of animal tunnels using 3D ground-penetrating radar. Near Surf. Geophys. 17, 291–298. https://doi.org/10.1002/nsg.12039.

Baccani, G., et al., 2018. The MIMA project. Design, construction and performances of a compact hodoscope for muon radiography applications in the context of archaeology and geophysical prospections. J. Instrum. 13 (11), P11001.

Bayoumi, A., Meguid, M.A., 2011. Wildlife and safety of earthen structures: a review. J. Fail. Anal. Prev. 11, 295–319. https://doi.org/10.1007/s11668-011-9439-y.

Bièvre, G., et al., 2018. Improvement of 2D ERT measurements conducted along a small earth-filled dyke using 3D topographic data and 3D computation of geometric factors. J. Appl. Geophys. 153, 100–112. https://doi.org/10.1016/j.jappgeo.2018.04.012.

Bonechi, L., D'Alessandro, R., Mori, N., et al., 2015. A projective reconstruction method of underground or hidden structures using atmospheric muon absorption data. J. Instrum. 10 (02), P02003.

Bonechi, L., Baccani, G., et al., 2020a. Multidisciplinary applications of muon radiography using the MIMA detector. J. Instrum. 15, C05030.

Bonechi, L., D'Alessandro, R., Giammanco, A., 2020b. Atmospheric muons as an imaging tool. Rev. Phys. 5, 100038.

Borgatti, L., et al., 2017. Detection and characterization of animal burrows within river embankments by means of coupled remote sensing and geophysical techniques: lessons from River Panaro (northern Italy). Eng. Geol. 226, 277–289. https://doi.org/10.1016/j.enggeo.2017.06.017.

Brierley, G.J., Ferguson, R.J., Woolfe, K.J., 1997. What is a fluvial levee? Sediment. Geol. 114, 1–9.

Busato, L., et al., 2016. Combined geophysical surveys for the characterization of a reconstructed river embankment. Eng. Geol. 211, 74–84. https://doi.org/10.1016/j.enggeo.2016.06.023.

Cardarelli, E., Cercato, M., De Donno, G., 2014. Characterization of an earth-filled dam through the combined use of electrical resistivity tomography; P- and SH-wave seismic tomography and surface wave data. J. Appl. Geophys. 106, 87–95. https://doi.org/10.1016/j.jappgeo.2014.04.007.

Chlaib, H.K., et al., 2014. Using ground penetrating radar in levee assessment to detect small scale animal burrows. J. Appl. Geophys. 103, 121–131. https://doi.org/10.1016/j.jappgeo.2014.01.011.

Cho, I.-K., Yeom, J.-Y., 2007. Crossline resistivity tomography for the delineation of anomalous seepage pathways in an embankment dam. Geophysics 72, G31–G38. https://doi.org/10.1190/1.2435200.

Dahlin, T., Zhou, B., 2004. A numerical comparison of 2D resistivity imaging with ten electrode arrays. Geophys. Prospect. 52, 379–398. https://doi.org/10.1111/j.1365-2478.2004.00423.x.

D'Errico, M., et al., 2020. Muon radiography applied to volcanoes imaging: the MURAVES experiment at Mt. Vesuvius. J. Instrum. 15, C03014. https://doi.org/10.1088/1748-0221/15/03/C03014.

Fishera, W.D., Campa, T.K., Krzhizhanovskaya, V.V., 2017. Anomaly detection in earth dam and levee passive seismic data using support vector machines and automatic feature selection. J. Comput. Sci. 20, 143–153. https://doi.org/10.1016/j.jocs.2016.11.016.

Ikard, S.J., Revil, A., et al., 2012. Saline pulse test monitoring with the self-potential method to non intrusively determine the velocity of the pore water in leaking areas of earth dams and embankments. Water Resour. Res. 48, W04201. https://doi.org/10.1029/2010WR010247.

Ikard, S.J., Rittgers, J., et al., 2015. Geophysical investigation of seepage beneath an earthen dam. Groundwater 53, 238–250. https://doi.org/10.1111/gwat.12185.

Lai, W.W.-L., Dérobert, X., Annan, P., 2018. A review of Ground Penetrating Radar application in civil engineering: A 30-year journey from Locating and Testing to Imaging and Diagnosis. NTD&E Int. 96, 58–78. https://doi.org/10.1016/j.ndteint.2017.04.002.

Loke, M.H., Barker, R.D., 1996. Practical techniques for 3D resistivity surveys and data inversion. Geophys. Prospect. 44, 499–523. https://doi.org/10.1111/j.1365-2478.1996.tb00162.x.

Moore, J.R., et al., 2011. Self-potential investigation of moraine dam seepage. J. Appl. Geophys. 74, 277–286. https://doi.org/10.1016/j.jappgeo.2011.06.014.

Morelli, S., Segoni, S., et al., 2012. Urban planning, flood risk and public policy: the case of the Arno River, Firenze, Italy. Appl. Geogr. 34, 205–218. https://doi.org/10.1016/j.apgeog.2011.10.020.

Morelli, S., Pazzi, V., et al., 2020. Characterization and geotechnical investigations of a riverbank failure in Florence, Italy, an UNESCO World Heritage Site. J. Geotech. Geoenviron. 146, 05020009. https://doi.org/10.1061/(ASCE)GT.1943-5606.0002305.

Niederleithinger, E., Weller, A., Lewis, R., 2012. Evaluation of geophysical techniques for dike inspection. J. Environ. Eng. Geophys. 17, 185–195. https://doi.org/10.2113/JEEG17.4.185.

Olivier, G., et al., 2017. Monitoring the stability of tailings dam walls with ambient seismic noise. Lead. Edge 36, 350a1–350a6. https://doi.org/10.1190/tle36040350a1.1.

Orlandini, S., Moretti, G., Albertson, J.D., 2015. Evidence of an emerging levee failure mechanism causing disastrous floods in Italy. Water Resour. Res. 51, 7995–8011. https://doi.org/10.1002/2015WR017426.

Panthulu, T.V., Krishnaiah, C., Shirke, J.M., 2001. Detection of seepage paths in earth dams using self-potential and electrical resistivity methods. Eng. Geol. 50, 281–295. https://doi.org/10.1016/j.jocs.2016.11.016.

Pazzi, V., Tapete, D., et al., 2016. An electric and electromagnetic geophysical approach for subsurface investigation of anthropogenic mounds in an urban environment. Geomorphology 273, 335–347. https://doi.org/10.1016/j.geomorph.2016.07.035.

Pazzi, V., Lotti, A., et al., 2017. Monitoring of the vibration induced on the Arno masonry embankment wall by the conservation works after the May 25, 2016 riverbank landslide. Geoenviron. Disast. 4, 6. https://doi.org/10.1186/s40677-017-0072-2.

Pazzi, V., Ceccatelli, M., Gracchi, T., et al., 2018a. Assessing subsoil void hazards along a road system using H/V measurements, ERTs, and IPTs to support local decision makers. Near Surf. Geophys. 16, 282–297. https://doi.org/10.3997/1873-0604.2018002.

Pazzi, V., Di Filippo, M., et al., 2018b. Integrated geophysical survey in a sinkhole-prone area: microgravity, electrical resistivity tomographies, and seismic noise measurements to delimit its extension. Eng. Geol. 243, 282–293. https://doi.org/10.1016/j.enggeo.2018.07.016.

Pazzi, V., Ceccatelli, M., Ciani, L., et al., 2020. Analysis of the influence of the GPS errors occurred while collecting electrode coordinates on the electrical resistivity of Tumuli. Sensors 20, 2966. https://doi.org/10.3390/s20102966.

PDG cap. 30, 2020. The Review of Particle Physics - Cosmic Rays. url: http://pdg.lbl.gov/2020/reviews/rpp2020-rev-cosmic-rays.pdf.

PDG cap. 34, 2020. The Review of Particle Physics - Passage of Particles Through Matter. url: http://pdg.lbl.gov/2020/reviews/rpp2020-rev-passage-particles-matter.pdf.

Perri, M.T., et al., 2014. River embankment characterization: the joint use of geophysical and geotechnical techniques. J. Appl. Geophys. 110, 5–22. https://doi.org/10.1016/j.jappgeo.2014.08.012.

Planès, T., et al., 2016. Time-lapse monitoring of internal erosion in earthen dams and levees using ambient seismic noise. Géotechnique 4, 301–312. https://doi.org/10.1680/jgeot.14.P.268.

Rittgers, J.B., et al., 2015. 4-D imaging of seepage in earthen embankments with time-lapse inversion of self-potential data constrained by acoustic emissions localization. Geophys. J. Int. 200, 756–770. https://doi.org/10.1093/gji/ggu432.

Santarato, G., et al., 2011. Three- dimensional electrical resistivity tomography to control the injection of expanding resins for the treatment and stabilization of foundation soils. Eng. Geol. 119, 18–30. https://doi.org/10.1016/j.enggeo.2011.01.009.

Szalai, S., Szarka, L., 2008. On the classification of surface geoelectric arrays. Geophys. Prospect. 56, 159–175. https://doi.org/10.1111/j.1365-2478.2007.00673.x.

The CGAL Project, 2020. CGAL User and Reference Manual. 5.0.2. CGAL Editorial Board url: https://doc.cgal.org/5.0.2/Manual/packages.html.

Viero, A., et al., 2015. Investigations on the structural setting of a landslide- prone slope by means of three-dimensional electrical resistivity tomography. Nat. Hazards 78, 1369–1385. https://doi.org/10.1007/s11069-015-1777-8.

Wilt, M.J., Corwin, R.F., 2005. Numerical modeling of self-potential anomalies due to leaky dams: Model and field examples. In: Merkler, G.P., et al. (Eds.), Detection of Subsurface Flow Phenomena. Lecture Notes in Earth Sciences. 27. Springer, Berlin, Heidelberg. https://doi.org/10.1007/BFb0011631.